

# A Low-Cost and Robust Maximum Likelihood Joint Estimator for the Doppler Spread and CFO Parameters Over Flat-Fading Rayleigh Channels

Faouzi Bellili, Yassine Selmi, Sofiène Affes, *Senior Member, IEEE*, and Ali Ghrayeb

**Abstract**—This paper addresses the problem of Doppler spread and carrier frequency offset (CFO) estimation under flat-fading Rayleigh channels. We develop a new low-cost and robust approximate maximum likelihood (ML) estimator for these two key parameters that builds upon an elegant two-ray approximation model of the channel's covariance matrix. The latter is then inverted analytically thereby yielding a closed-form expression for the underlying log-likelihood function that is prone to easy evaluation by the fast Fourier transform. Computer simulations show that the new estimator is accurate over wide ranges of the Doppler spread and CFO parameters. Moreover, it outperforms many state-of-the-art techniques under the adverse conditions of short data records and/or low SNR thresholds. Most prominently, it exhibits an unprecedented robustness to the Doppler spectrum shape of the channel since it does not require its *a priori* knowledge.

**Index Terms**—Doppler spread estimation, CFO estimation, maximum likelihood, Rayleigh channels.

## I. INTRODUCTION

CARRIER synchronization is a crucial task in any digital communication system. In fact, due to inevitable hardware imperfections and aging effects, the communication link is often subject to a carrier frequency offset (CFO) between transceivers' local oscillators. If not accurately estimated and compensated, the CFO leads to severe performance degradation even in the presence of powerful error-correcting codes. Early solutions for the CFO mitigation under constant channels relied on automatic frequency tracking loop at the receiver (see [2], [3] and references therein). However, the rapid advances in microelectronics and microprocessors made the implementation of sophisticated algorithms feasible in base-band. In this context, frequency synchronization schemes based on CFO estimation/compensation have attracted a

lot of research interest and many CFO estimators have been introduced in the open literature for different system architectures [4]– [9]. But, most of the proposed techniques rely on the simplifying assumption of constant channels. A fairly exhaustive survey and classification of the various techniques proposed during the last five years can be found in [10] wherein the emphasis is put on the advantages and drawbacks of each technique. In particular, the ML estimator first formulated in [11] shows that the CFO estimate can be easily obtained by taking the DFT of the received samples. Many enhanced versions based on this simple observation were proposed later (see [12]– [14] and references therein).

Furthermore, current and future-generation systems such as long-term-evolution (LTE), LTE-Advanced (LTE-A) and beyond (LTE-B) are expected to support reliable communications at very high velocities reaching 500 Km/h [15]. For such systems, classical assumptions of constant channels no longer hold thereby leading to severe performance degradation of the existing CFO estimation approaches. More specifically, the transmitter/receiver motion introduces a Doppler spread which smears the spectral content of the channel and one needs to account for such Doppler effects during the CFO estimation process. In other words, a particular challenge for frequency estimation under time-selective channels is that, in addition to the additive noise, the transmitted signal becomes corrupted by a randomly time-variant (TV) multiplicative distortion (MD).

In this context, a number of CFO estimation techniques accounting for the TV MD have been reported in the open literature. But most of them are either correlation- or periodogram-based solutions [16]– [21]. Hence, they suffer from severe performance degradation in adverse conditions of short data records and/or low SNR levels. Moreover, except for [20], all these methods require the unpractical knowledge of the Doppler spectrum shape during the estimation process. ML-based approaches, however, are well known to provide the best performance under the aforementioned harsh conditions. Yet, it was only recently that ML CFO estimation under time-varying channels has been addressed: *i*) for single carrier systems in [22] where the well-known auto-regressive (AR) model was leveraged to find an approximate ML solution (under the very special case of uniform Jakes' model), and *ii*) for multicarrier systems in [23] and [24].

From another perspective, most of the existing solutions assume the Doppler spread (or equivalently the maximum Doppler shift) to be perfectly known during the CFO estimation process (see [25]– [28] and references therein). This is

Manuscript received November 2, 2016; revised March 7, 2017; accepted April 14, 2017. Date of publication April 25, 2017; date of current version August 14, 2017. This work was made possible by NPRP grant NPRP 5-250-2-087 from the Qatar National Research Fund (a member of Qatar Foundation). The statements made herein are solely the responsibility of the authors. The associate editor coordinating the review of this paper and approving it for publication was Y.-C. Wu. (*Corresponding author: Faouzi Bellili.*)

F. Bellili is with The Edward S. Rogers Sr. Department of Electrical and Computer Engineering, University of Toronto, Toronto, ON M5S 3G4, Canada (e-mail: faouzi.bellili@utoronto.ca).

Y. Selmi and S. Affes are with INRS-EMT, Montreal, QC H5A 1K6, Canada (e-mail: yassine.selmi@emt.inrs.ca; affes@emt.inrs.ca).

A. Ghrayeb is with Texas A&M University at Qatar, Doha 23874, Qatar (e-mail: ali.ghrayeb@qatar.tamu.edu).

Color versions of one or more of the figures in this paper are available online at <http://ieeexplore.ieee.org>.

Digital Object Identifier 10.1109/TCOMM.2017.2697962

another restrictive assumption since, in practice, the Doppler spread is usually unknown and needs to be estimated online as well. More so, the Doppler spread itself is another key parameter for transceiver optimization designs. For instance, it is used to optimize the feedback rate of channel state information (CSI)-based schemes [29]. The Doppler spread estimate is also required to optimize the power control and handoff schemes [30], [31], as well as, the adaptation step of adaptive channel identification algorithms [32]. Moreover, due to the very nature of the newly deployed heterogeneous networks (HetNets), the well-known interference mitigation and handoff hysteresis issues are exacerbated when a moving user temporarily enters or even approaches a small cell (i.e., picos or femtos), thereby interfering with its users and possibly resulting in brief macro/small and small/macro cell-reassignments [33]. Reducing interference and avoiding useless handoffs can be achieved by predicting the evolution of the interferer's trajectory through its Doppler spread information; that is its instantaneous velocity.

Depending on how the observation data are processed, four classes of Doppler estimators [34], [35] are encountered in the open literature: level-crossing rate (LCR)-based [36], [37], covariance-based [38] – [40], spectrum-based [41], and ML-based techniques. The covariance-based estimators are usually preferred against LCR-based ones which require larger-size observation windows. Otherwise, the number of crossings may be very small or there may even be no crossings at all for small Doppler values. The performance of the covariance-based estimators themselves degrades drastically for a relatively small number of received samples, due to weak averaging effects (i.e., unreliable estimates of the channel autocorrelation coefficients). The spectrum-based techniques inherit the same limitations since the channel's spectrum is nothing but the discrete-time Fourier transform of its autocorrelation coefficients. For the very same reasons put forward in CFO estimation, ML Doppler estimation is preferred as long as it is computationally manageable.

To the best of our knowledge, five ML-based Doppler estimators have been so far introduced in the open literature. One of the first implementations of the ML criterion was proposed in [42] whose basic idea is to maximize the similarity between the power spectral density (PSD) of the received signal and a hypothetical one (namely the uniform Jakes' model). Another early ML approach was also introduced in [43], in the specific context of TDMA transmissions, wherein periodic pilot symbols are transmitted over each time slot. It involves, however, the numerical inversion of a large-size covariance matrix, a quite computationally-demanding operation in practice. Another ML Doppler estimator was developed in [44] using the Whittle approximation. However, it works only for very large normalized Doppler frequencies (typically  $f_n > 0.1$  where  $f_n = f_D T_s$  and  $T_s$  is the symbol period). The most recent ML estimator was proposed in [22] by exploiting an AR model (of order one) is unable to capture small Doppler values as well as will be seen later in Section IV. Actually, estimating very small normalized Doppler frequencies is more challenging yet of much interest in practice. Indeed, current 4G wireless communication systems and beyond are characterized

by high-data-rate transmissions and, hence, require very small symbol periods (typically  $T_s \approx 10 \mu\text{s}$  over each subcarrier in LTE systems [45]). Hence, the target normalized Doppler frequencies for these systems are typically in the range of  $0.0001 \leq f_n \leq 0.01$  for a maximum Doppler frequency  $f_D$  ranging from 1 to 1000 Hz. This translates to a user velocity  $v = \frac{f_D}{F_0} c$  ranging between 5.4 Km/h and 540 Km/h at a carrier frequency  $F_0 = 2$  GHz ( $c$  being the speed of light). The only two estimators that were specifically designed to cope with relatively small normalized Doppler frequencies are TAML [46] and COMAT [47]. TAML is an ML-based approach that, despite avoiding the inversion of the true covariance matrix, incurs a very high computational cost in practice. Indeed it relies on the approximation of the actual channel correlation matrix by a Taylor series of order  $K$ . Consequently, it involves the numerical inversion of a  $(K \times K)$  matrix at each point of the search grid (where  $K$  is in the order of 10) on the top of several other matrix multiplications. COMAT, however, is a covariance-matching approach that is computationally more attractive but requires large-size data records to capture small Doppler spread values. Another limitation of all the Doppler estimators discussed above [42]–[47] is that they all assume the perfect *a priori* knowledge of the channel spectrum form and most of them were specifically designed for the very special case of the *uniform Jakes'* model.

Motivated by all these facts, we develop in this paper a new ML joint estimator for both the CFO and the Doppler spread that:

- involves no matrix manipulations (i.e., inversion or multiplication) thereby resulting in a huge computational saving;
- does not require any *a priori* knowledge about the channel's power spectral density (PSD) and is robust to its shape;
- is able to accurately estimate extremely small Doppler frequencies.

The new estimator reduces the log-likelihood function (LLF) into the orthogonal projection of the observation vector onto a two-dimensional subspace that can be easily evaluated by FFT. It is also based on a second-order Taylor expansion series that is valid for most known channel PSD models, including the very basic and widely studied *uniform Jakes*, *restricted Jakes* (rJakes), Gaussian, biGaussian, rounded, bell, and 3-D flat models, etc. Exhaustive computer simulations show that the new ML approach outperforms the main state-of-art techniques both in CFO and Doppler estimation, more so in the adverse conditions stemming from short data records and/or small SNR levels.

We organize the rest of this paper as follows. In section II, we introduce the system model. In section III, we develop our new ML estimator. In section IV, we assess its performance and compare it against the main state-of-the-art techniques. Finally, we draw out some concluding remarks in section V.

We define in the following the adopted mathematical notations: Vectors and matrices are represented in lower- and upper-case bold fonts, respectively.  $\mathbf{I}_N$ ,  $\mathbf{1}_N$ , and  $\mathbf{0}_N$  denote the  $N \times N$  identity matrix, the all-one, and the all-zero  $N$ -dimensional vectors, respectively. The Hadamard product

of any two matrices  $\mathbf{A}$  and  $\mathbf{B}$  (i.e., elementwise product) is denoted as  $\mathbf{A} \odot \mathbf{B}$  and  $\det\{\cdot\}$  returns the determinant of any square matrix. Moreover,  $\{\cdot\}^T$  and  $\{\cdot\}^H$  denote the transpose and the Hermitian (transpose conjugate) operators, respectively. The Euclidean norm of a vector is denoted as  $\|\cdot\|$  and  $\text{diag}\{x_1, x_2, \dots, x_n\}$  is the diagonal matrix whose main diagonal is composed of the entries  $x_1, x_2, \dots, x_n$  in the given order. The operators  $\{\cdot\}^*$  and  $|\cdot|$  return the conjugate and magnitude of any complex number, respectively, and  $j$  is the unit complex constant,  $j^2 = -1$ . We also use  $(\cdot)$  and  $[\cdot]$  for continuous and discrete variables, respectively. Finally, the statistical expectation is denoted as  $\mathbb{E}\{\cdot\}$  and  $\triangleq$  is used for definitions.

## II. SYSTEM MODEL

Consider a reference (i.e., known) signal,  $x(t)$ , that is transmitted over a flat-fading Rayleigh channel,  $h(t)$ . In the presence of a CFO,  $f_c$ , the baseband-equivalent received signal, after down conversion, is given by [47]:

$$y(t) = h(t)x(t)e^{j2\pi f_c t} + w(t), \quad (1)$$

where  $w(t)$  is an additive noise modeled by a zero-mean complex circular white Gaussian random process. Sampling  $y(t)$  at the rate  $f_s = 1/T_s$  and assuming without loss of generality that  $x(t) = 1 \forall t$  yields the following discrete-time observation data sequence:

$$y[n] = h[n]e^{j2\pi n f_c T_s} + w[n], \quad n = 0, 1, \dots, N-1, \quad (2)$$

where  $y[n] = y(nT_s)$ ,  $h[n] = h(nT_s)$ , and  $w[n] = w(nT_s)$ . Here, we do not assume that the transmitted signal propagates along a *single path* to the receiver. Rather, we consider a single-tap model for the baseband-equivalent representation of the physical *multipath channel*. Actually, if the wireless channel were composed of a single path (a situation that is rarely encountered in practice), then there would be no Doppler spread, but a simple Doppler shift that can be easily incorporated in the CFO in (1). However, although wireless physical channels are usually multipath, they can be modelled in the baseband domain either by a single-tap or a multi-tap model depending on how the channel's coherence bandwidth,  $B_c$ , compares to the sampling rate,  $f_s$ , which is assumed to be equal to the Nyquist rate of the transmitted reference signal. In either case, a tap is composed of an aggregation over all physical paths that cannot be resolved in the delay line. Each of these unresolvable paths has its own Doppler shift and, collectively, they result in the so-called Doppler spread of the tap to which they belong. More explicitly, we have the following two different conditions:

- $B_c > f_s = \frac{1}{T_s} \implies$  the baseband-equivalent model for the physical multipath channel is composed of a single tap; this is widely referred to as flat-fading/narrowband model.
- $B_c < f_s = \frac{1}{T_s} \implies$  the baseband-equivalent model for the physical multipath channel is composed of more than one tap; this is widely referred to as frequency-selective/wideband model.

In our work, we are under the first condition (i.e., the flat-fading scenario) wherein all the physical paths contribute to a single tap. Such narrowband model is well justified in practice by its wide adoption in current and next-generation multicarrier communication systems such as long-term-evolution (LTE), LTE-advanced (LTE-A) and beyond (LTE-B) systems. In fact, it is well known that OFDM systems transform a multipath frequency-selective channel in the time domain into a frequency-flat (i.e., narrowband) channel over each subcarrier. Actually, multicarrier technologies were primarily designed to combat the multipath effects in high-data-rate communications by bringing back the per-carrier propagation channel to the simple flat-fading case [48], [49].

In the rest of this paper, the estimation problem is formulated as follows: Given the  $N$  data records in (2), our goal is to estimate the Doppler spread (or equivalently the maximum Doppler frequency) jointly with the CFO. Note that although the model in (2) is expressed explicitly in terms of the CFO, the Doppler spread is hidden in the channel's autocorrelation coefficients given by:

$$r_h[k] \triangleq \mathbb{E} \left\{ h[n]h[n+k]^* \right\}, \quad k \in \mathbb{Z}. \quad (3)$$

For instance, in the very specific case of *uniform Jakes'* model,  $r_h(kT_s)$  is given by:

$$r_h[k] = J_0(2\pi k f_D T_s) = J_0(\sqrt{2}k\sigma_D T_s),$$

where  $J_0(\cdot)$  is the zero-order Bessel function of the first kind and the second equality follows from the relationship between the maximum Doppler frequency,  $f_D$ , and the Doppler spread,  $\sigma_D$ , in the *uniform Jakes* model:

$$\sigma_D = \frac{2\pi}{\sqrt{2}} f_D. \quad (4)$$

The *uniform Jakes'* model is assumed in typical urban environments where the multipath components tend to hit the receiver from almost all the directions uniformly. In practice, however, other models can be encountered, depending on the distribution of the angles of arrivals (AoAs) of the incoming signal. This gives rise to other Doppler spectra such as the 3D-flat, rounded, Gaussian, Bi-Gaussian, symmetrical restricted Jakes (rJakes), asymmetrical Jakes (aJakes) models, etc. The explicit relationship between  $\sigma_D$  and  $f_D$  for each of the aforementioned models can be obtained from the following general identity:

$$\sigma_D = \left( \frac{1}{2\pi} \int_{-\omega_D}^{\omega_D} \omega^2 S(\omega) d\omega \right)^{1/2} \quad \text{with} \quad \omega_D = 2\pi f_D. \quad (5)$$

Here,  $S(\omega)$  is the PSD of the channel, i.e., the discrete-time Fourier transform of its autocorrelation coefficients defined in (3):

$$S(\omega) \triangleq \sum_{k=-\infty}^{+\infty} r_h[k] e^{-jk\omega}. \quad (6)$$

For instance, for the 3-D scattering model (i.e., flat PSD), it can be shown using the relationship in (5) that the Doppler

spread and the maximum Doppler frequency are related as follows:

$$\sigma_D = \frac{2\pi}{\sqrt{3}} f_D. \quad (7)$$

As mentioned in Section I, a distinct advantage of the new ML estimator is its capability of estimating the Doppler spread with almost all known models without even knowing its PSD form. For mathematical convenience, we now introduce the following vector notations:

$$\begin{aligned} \mathbf{y} &\triangleq [y[0], y[1], \dots, y[N-1]]^T, \\ \mathbf{h} &\triangleq [h[0], h[1], \dots, h[N-1]]^T, \\ \mathbf{w} &\triangleq [w[0], w[1], \dots, w[N-1]]^T. \end{aligned}$$

Hence, the model in (2) can be rewritten in the following more compact matrix/vector form:

$$\mathbf{y} = \Phi(\omega_c)\mathbf{h} + \mathbf{w}, \quad (8)$$

where  $\omega_c \triangleq 2\pi f_c$  and  $\Phi(\omega)$  is a diagonal matrix defined for any (unnormalized) angular frequency  $\omega = 2\pi f$  as follows

$$\Phi(\omega) \triangleq \text{diag}\{1, e^{j\omega T_s}, e^{j2\omega T_s}, \dots, e^{j(N-1)\omega T_s}\}. \quad (9)$$

### III. FORMULATION OF THE NEW ML ESTIMATOR

To begin with, we stack the unknown parameters of interest in a single parameter vector denoted as  $\boldsymbol{\theta} \triangleq [\sigma_D, f_c]^T$ . A key step in the derivation of ML estimators consists in finding the LLF,  $\mathcal{L}_y(\boldsymbol{\theta})$ , of the estimation problem at hand defined as:

$$\mathcal{L}_y(\boldsymbol{\theta}) \triangleq \log(p(\mathbf{y}; \boldsymbol{\theta})), \quad (10)$$

where  $p(\mathbf{y}; \boldsymbol{\theta})$  is the probability density function (pdf) of the observation data vector,  $\mathbf{y}$ , parameterized by  $\boldsymbol{\theta}$ . Owing to (8), it can be shown that  $\mathbf{y}$  is a circular symmetric Gaussian random vector with zero mean. Therefore, we have:

$$p(\mathbf{y}; \boldsymbol{\theta}) = \frac{1}{\pi^N \det\{\mathbf{R}_y(\boldsymbol{\theta})\}} \exp\{-\mathbf{y}^H \mathbf{R}_y^{-1}(\boldsymbol{\theta}) \mathbf{y}\}, \quad (11)$$

where  $\mathbf{R}_y(\boldsymbol{\theta}) \triangleq \mathbb{E}\{\mathbf{y}\mathbf{y}^H\}$  is the covariance matrix of  $\mathbf{y}$ . From (8), it is also easy to show that:

$$\mathbf{R}_y(\boldsymbol{\theta}) \triangleq \Phi(\omega_c) \mathbf{R}_h(\sigma_D) \Phi(\omega_c)^H + \sigma_n^2 \mathbf{I}_N, \quad (12)$$

in which  $\mathbf{R}_h(\sigma_D) \triangleq \mathbb{E}\{\mathbf{h}\mathbf{h}^H\}$  is the covariance matrix of the channel. Now, taking the logarithm of (11) and dropping the constant terms yields the LLF as:

$$\mathcal{L}_y(\boldsymbol{\theta}) = -\log(\det\{\mathbf{R}_y(\boldsymbol{\theta})\}) - \mathbf{y}^H \mathbf{R}_y^{-1}(\boldsymbol{\theta}) \mathbf{y}. \quad (13)$$

At this early stage, the true challenge of the ML derivation is obvious. Indeed, maximizing  $\mathcal{L}_y(\boldsymbol{\theta})$  with respect to the unknown parameter vector,  $\boldsymbol{\theta}$ , requires from (13) the inversion of a large-size ( $N \times N$ ) covariance matrix and the computation of its determinant. Hence, its computational complexity, in the order of  $O(N^3)$  operations, increases very quickly with  $N$  (e.g.,  $10^6$  operations at each point of the search grid even for a relatively small  $N = 100$  samples). This suggests that any naive implementation of the ML estimator would be simply too prohibitive in complexity. To avoid the inversion of a large-size covariance matrix, Tsai and Young have recently proposed

in [46] an approximate LLF (in the absence of CFO) using a  $K$ -order Taylor series expansion of the channel's correlation function. The resulting approximate ML Doppler estimator of [46] requires only the inversion of a ( $K \times K$ ) matrix no matter how large is  $N$  where  $K \ll N$  ( $K$  is typically in the range of 10). However, it still requires a series of heavy multiplications of ( $K \times K$ ) matrices on the top of the matrix inversion. Also, the reduced-size approximate matrix — being badly conditioned — results in numerical instabilities. We will further discuss this limitation later in Section IV.

In this paper, we propose a new approximate ML solution that avoids any matrix inversion or multiplication, thereby resulting in a huge computational saving. We rely on the following second-order Taylor series approximation of the covariance matrix, developed in [47], which is valid for most known Doppler PSD models:

$$\mathbf{R}_h(\sigma_D) = \frac{\sigma_h^2}{2} \mathbf{A}(\sigma_D) \mathbf{A}^H(\sigma_D). \quad (14)$$

In (14), the matrix  $\mathbf{A}(\omega)$  is defined for any angular frequency  $\omega$  as follows:

$$\mathbf{A}(\omega) = [\mathbf{a}(-\omega) \quad \mathbf{a}(\omega)], \quad (15)$$

in which the vector  $\mathbf{a}(\omega)$  is defined as:

$$\mathbf{a}(\omega) \triangleq [1 \quad e^{j\omega T_s} \quad e^{j2\omega T_s} \quad \dots \quad e^{j(N-1)\omega T_s}]^T. \quad (16)$$

After plugging (14) back into (12), an approximate expression for the overall covariance matrix of the observation vector is obtained as:

$$\mathbf{R}_y(\boldsymbol{\theta}) = \frac{\sigma_h^2}{2} \Phi(\omega_c) \mathbf{A}(\sigma_D) \mathbf{A}^H(\sigma_D) \Phi(\omega_c)^H + \sigma_n^2 \mathbf{I}_N. \quad (17)$$

In our quest for finding the analytical inverse of the ( $N \times N$ ) covariance matrix,  $\mathbf{R}_y(\boldsymbol{\theta})$ , and its determinant, we begin by finding the analytical expressions of the non-zero eigenvalues of the matrix  $\mathbf{A}(\sigma_D) \mathbf{A}(\sigma_D)^H$  and their associated eigenvectors. Actually, this matrix is of rank two and as such has two nonzero eigen-values only. Further, it is known from basic linear algebra that the non-zero eigenvalues of  $\mathbf{A}(\sigma_D) \mathbf{A}(\sigma_D)^H$  and  $\mathbf{A}(\sigma_D)^H \mathbf{A}(\sigma_D)$  are the same. Fortunately, the latter matrix is of size  $2 \times 2$  and, thus, its eigen-values can be found analytically. Indeed, it is easy to establish that:

$$\mathbf{A}(\sigma_D)^H \mathbf{A}(\sigma_D) = \begin{pmatrix} \|\mathbf{a}(-\sigma_D)\|^2 & \mathbf{a}(-\sigma_D)^H \mathbf{a}(\sigma_D) \\ \mathbf{a}(\sigma_D)^H \mathbf{a}(-\sigma_D) & \|\mathbf{a}(\sigma_D)\|^2 \end{pmatrix}. \quad (18)$$

Furthermore, it can be easily shown that  $\|\mathbf{a}(-\sigma_D)\|^2 = \|\mathbf{a}(\sigma_D)\|^2 = N$  and that:

$$\mathbf{a}(-\sigma_D)^H \mathbf{a}(\sigma_D) = \varphi(2\sigma_D T_s), \quad (19)$$

where

$$\varphi(x) \triangleq \sum_{n=0}^{N-1} e^{jn x} = \frac{\sin(\frac{Nx}{2})}{\sin(\frac{x}{2})} e^{j\frac{N-1}{2}x}, \quad (20)$$

is the Dirichlet Kernel. Consequently, the matrix  $\mathbf{A}(\sigma_D)^H \mathbf{A}(\sigma_D)$  in (18) is explicitly given by:

$$\mathbf{A}(\sigma_D)^H \mathbf{A}(\sigma_D) = \begin{pmatrix} N & \varphi(2\sigma_D T_s) \\ \varphi(2\sigma_D T_s)^* & N \end{pmatrix}. \quad (21)$$

The two eigenvalues,  $\lambda_1$  and  $\lambda_2$ , of this matrix are the roots of the corresponding characteristic polynomial given by:

$$\begin{aligned} \mathcal{P}(\lambda) &\triangleq \det \left\{ \lambda \mathbf{I} - \mathbf{A}(\sigma_D)^H \mathbf{A}(\sigma_D) \right\} \\ &= (\lambda - N)^2 - |\varphi(2\sigma_D T_s)|^2. \end{aligned}$$

Setting  $\mathcal{P}(\lambda) = 0$  and solving for  $\lambda$  leads to:

$$\lambda_1(\sigma_D) = N + \left| \frac{\sin(N\sigma_D T_s)}{\sin(\sigma_D T_s)} \right|, \quad (22)$$

$$\lambda_2(\sigma_D) = N - \left| \frac{\sin(N\sigma_D T_s)}{\sin(\sigma_D T_s)} \right|. \quad (23)$$

Moreover, by closely inspecting (21), it can be easily shown that:

$$\mathbf{v}_1(\sigma_D) = \frac{1}{\sqrt{2}} \begin{bmatrix} 1 & \frac{\varphi(2\sigma_D T_s)^*}{|\varphi(2\sigma_D T_s)|} \end{bmatrix}^T \quad (24)$$

$$\mathbf{v}_2(\sigma_D) = \frac{1}{\sqrt{2}} \begin{bmatrix} 1 & -\frac{\varphi(2\sigma_D T_s)^*}{|\varphi(2\sigma_D T_s)|} \end{bmatrix}^T. \quad (25)$$

are two unit-norm eigenvectors of  $\mathbf{A}(\sigma_D)^H \mathbf{A}(\sigma_D)$  associated to  $\lambda_1(\sigma_D)$  and  $\lambda_2(\sigma_D)$ , respectively. Recall here that  $\lambda_1(\sigma_D)$  and  $\lambda_2(\sigma_D)$  are also the only two non-zero singular values of the  $(N \times N)$  matrix of interest  $\mathbf{A}(\sigma_D) \mathbf{A}(\sigma_D)^H$ . We are now ready to find its two unit-norm eigenvectors,  $\mathbf{u}_1(\sigma_D)$  and  $\mathbf{u}_2(\sigma_D)$ , that are associated to  $\lambda_1$  and  $\lambda_2$ , respectively. To do so, let the economy-size singular value decomposition (SVD) of the matrix  $\mathbf{A}(\sigma_D)$  be:

$$\mathbf{A}(\sigma_D) = \mathbf{U}(\sigma_D) \Sigma(\sigma_D)^{1/2} \mathbf{V}(\sigma_D)^H, \quad (26)$$

with

$$\mathbf{U}(\sigma_D) \triangleq [\mathbf{u}_1(\sigma_D) \quad \mathbf{u}_2(\sigma_D)] \quad (27)$$

$$\mathbf{V}(\sigma_D) \triangleq [\mathbf{v}_1(\sigma_D) \quad \mathbf{v}_2(\sigma_D)] \quad (28)$$

$$\Sigma(\sigma_D) \triangleq \text{diag}\{\lambda_1(\sigma_D), \lambda_2(\sigma_D)\}. \quad (29)$$

Then, exploiting the fact that  $\mathbf{V}(\sigma_D)^H \mathbf{V}(\sigma_D) = \mathbf{I}_2$ , it immediately follows from (26) that  $\mathbf{U}(\sigma_D)$  is expressed as:

$$\mathbf{U}(\sigma_D) = \mathbf{A}(\sigma_D) \mathbf{V}(\sigma_D) \Sigma(\sigma_D)^{-1/2}, \quad (30)$$

from which it can be shown that  $\mathbf{u}_1(\sigma_D)$  and  $\mathbf{u}_2(\sigma_D)$  are explicitly given by:

$$\mathbf{u}_1(\sigma_D) = \frac{1}{\sqrt{2\lambda_1(\sigma_D)}} \left( \mathbf{a}(-\sigma_D) + \frac{\varphi(2\sigma_D T_s)^*}{|\varphi(2\sigma_D T_s)|} \mathbf{a}(\sigma_D) \right), \quad (31)$$

$$\mathbf{u}_2(\sigma_D) = \frac{1}{\sqrt{2\lambda_2(\sigma_D)}} \left( \mathbf{a}(-\sigma_D) - \frac{\varphi(2\sigma_D T_s)^*}{|\varphi(2\sigma_D T_s)|} \mathbf{a}(\sigma_D) \right). \quad (32)$$

From (26), we also have:

$$\mathbf{A}(\sigma_D) \mathbf{A}(\sigma_D)^H = \mathbf{U}(\sigma_D) \Sigma(\sigma_D) \mathbf{U}(\sigma_D)^H. \quad (33)$$

By injecting (33) back into (17), the approximate covariance matrix of the observation vector develops into:

$$\mathbf{R}_y(\boldsymbol{\theta}) = \sigma_n^2 \left( \frac{\rho}{2} \mathbf{B}(\boldsymbol{\theta}) \Sigma(\sigma_D) \mathbf{B}(\boldsymbol{\theta})^H + \mathbf{I}_N \right), \quad (34)$$

in which  $\rho \triangleq \sigma_h^2 / \sigma_n^2$  is the average SNR of the system and the matrix  $\mathbf{B}(\boldsymbol{\theta})$  is defined as follows:

$$\mathbf{B}(\boldsymbol{\theta}) \triangleq \Phi(\omega_c) \mathbf{U}(\sigma_D). \quad (35)$$

For the sake of simplicity, we will temporarily rid in the upcoming derivations any matrix/vector parameterized notation-wise by  $\boldsymbol{\theta}$ ,  $\sigma_D$ , or  $\omega_c$  from their arguments until we establish at the very end the LLF expression. Now, applying the Woodbury identity (usually known as the matrix inversion lemma [50]) to (34) it can be shown that:

$$\mathbf{R}_y^{-1} = \frac{1}{\sigma_n^2} \left[ \mathbf{I} - \mathbf{B} \left( \frac{2}{\rho} \Sigma^{-1} + \mathbf{B}^H \mathbf{B} \right)^{-1} \mathbf{B}^H \right]. \quad (36)$$

Moreover, it can be easily verified that  $\mathbf{u}_1$  and  $\mathbf{u}_2$  are orthogonal and have unit norms thereby leading to  $\mathbf{U}^H \mathbf{U} = \mathbf{I}_2$ . Hence, recalling (35) and using the fact that  $\Phi^H \Phi = \mathbf{I}_N$ , we also have  $\mathbf{B}^H \mathbf{B} = \mathbf{U}^H \Phi^H \Phi \mathbf{U} = \mathbf{I}_2$ . Consequently, (36) reduces simply to:

$$\mathbf{R}_y^{-1} = \frac{1}{\sigma_n^2} \left( \mathbf{I} - \mathbf{B} \mathbf{A} \mathbf{B}^H \right), \quad (37)$$

in which  $\mathbf{A} \triangleq \left( \frac{2}{\rho} \Sigma^{-1} + \mathbf{I} \right)^{-1}$  is explicitly given by:

$$\mathbf{A} = \text{diag} \left\{ \frac{\rho \lambda_1}{2 + \rho \lambda_1}, \frac{\rho \lambda_2}{2 + \rho \lambda_2} \right\}. \quad (38)$$

By revisiting (34), it can also be shown that the eigenvalues of  $\mathbf{R}_y$ , denoted hereafter as  $\{\lambda'_l\}_{l=1}^N$ , are given by:

$$\lambda'_1 = \sigma_n^2 (\rho \lambda_1 + 2) / 2, \quad (39)$$

$$\lambda'_2 = \sigma_n^2 (\rho \lambda_2 + 2) / 2, \quad (40)$$

$$\lambda'_l = \sigma_n^2, \quad (\text{for } l = 3, 4, \dots, N). \quad (41)$$

Therefore, the determinant of  $\mathbf{R}_y$ , which is the product of its eigenvalues, can be readily obtained as:

$$\det \{\mathbf{R}_y\} = \frac{\sigma_n^{2N}}{4} (2 + \rho \lambda_1) (2 + \rho \lambda_2). \quad (42)$$

Finally, substituting (37) and (42) back into (13) and dropping the constant terms (that do not depend on the unknown Doppler spread and CFO), the LLF reduces simply to:

$$\mathcal{L}_y(\boldsymbol{\theta}) = -\log \left( [2 + \rho \lambda_1][2 + \rho \lambda_2] \right) + \frac{1}{\sigma_n^2} \left\| \Lambda^{1/2} \mathbf{B}^H \mathbf{y} \right\|^2. \quad (43)$$

This approximate likelihood expression involves the noise variance,  $\sigma_n^2$ , and the SNR,  $\rho$ , which are also unknown parameters in practice. In this work, they are estimated by a technique<sup>1</sup> that capitalizes on the fact that the approximate covariance matrix of the channel is of rank two [47]. Indeed, we form a  $(p \times p)$  Toeplitz matrix,  $\mathbf{R}_y^{(p)}$ , constructed from the first  $p$  ( $p \ll N$ ) estimated correlation coefficients,  $\{\hat{r}_y[k]\}_{k=1}^p$ , of  $\{y[n]\}_{n=0}^{N-1}$ . On the one hand, owing to (41), the

<sup>1</sup>Note here that other more elaborate data-aided (DA) techniques could be used to estimate the required noise variance and *instantaneous* SNR, e.g., [51] and [52].

$p - 2$  smallest eigenvalues of  $\mathbf{R}_y^{(p)}$  are nothing but multiple estimates of the unknown noise variance. Therefore, they can be averaged together to obtain a more refined estimate,  $\hat{\sigma}_n^2$ , of  $\sigma_n^2$ . On the other hand, since the zero-lag correlation coefficient is given by  $r_y[0] = \sigma_n^2 + \sigma_n^2$ , then the channel power is estimated as  $\hat{\sigma}_n^2 = \hat{r}_y[0] - \hat{\sigma}_n^2$ . The SNR estimate is then obtained as  $\hat{\rho} = \hat{\sigma}_n^2 / \hat{\sigma}_n^2$ . By injecting these estimates in (43), expanding the norm, and recalling (35), the LLF develops into:

$$\mathcal{L}_y(\boldsymbol{\theta}) = -\log(\psi(\sigma_D)) + \frac{1}{\hat{\sigma}_n^2} \sum_{i=1}^2 \gamma_i(\sigma_D)^2 \left| \mathbf{u}_i(\sigma_D)^H \boldsymbol{\Phi}(\omega_c)^H \mathbf{y} \right|^2, \quad (44)$$

in which:

$$\psi(\sigma_D) = [2 + \hat{\rho} \lambda_1(\sigma_D)][2 + \hat{\rho} \lambda_2(\sigma_D)], \quad (45)$$

$$\gamma_i(\sigma_D) = \sqrt{\frac{\hat{\rho} \lambda_i(\sigma_D)}{2 + \hat{\rho} \lambda_i(\sigma_D)}}, \quad i = 1, 2. \quad (46)$$

Then ML estimates of the Doppler spread and the CFO, respectively,  $\hat{\boldsymbol{\theta}} = [\hat{\sigma}_d, \hat{f}_c]$ , are then obtained as:

$$\hat{\boldsymbol{\theta}} = \arg \max_{\boldsymbol{\theta}} \mathcal{L}_y(\boldsymbol{\theta}). \quad (47)$$

We emphasize here the fact that the final LLF expression in (44) does not involve any matrix inverse. Moreover, to side-step the remaining matrix multiplication in (44) and speed up the execution time in practice, the following two remarks are in order:

• *Remark 1:* The second term in the LLF can be easily computed by the FFT at each candidate Doppler value over the postulated search grid. In fact, by denoting the  $n^{\text{th}}$  element of the vector  $\mathbf{u}_i(\sigma_D)$  as  $u_{i,\sigma_D}(n)$  for  $i = 1, 2$ , it can be shown that:

$$\mathbf{u}_i(\sigma_D)^H \boldsymbol{\Phi}(\omega_c)^H \mathbf{y} = \sum_{n=0}^{N-1} u_{i,\sigma_D}(n)^* y(n) e^{-jn\omega_c T_s} = \tilde{z}_{i,\sigma_D}(\omega_c),$$

where  $\tilde{z}_{i,\sigma_D}(\omega_c)$  is the discrete-time Fourier transform (DTFT) of the sequence  $\{z_{i,\sigma_D}(n)\}_{n=0}^{N-1}$  defined for  $i = 1, 2$  as follows:

$$z_{i,\sigma_D}(n) \triangleq u_{i,\sigma_D}(n)^* y(n). \quad (48)$$

Therefore, in order to evaluate the LLF,  $\mathcal{L}(\boldsymbol{\theta}) = \mathcal{L}(\sigma_D, \omega_c)$  at all candidate values,  $\{\omega_c^{(m)}\}_{m=1}^M$ , of  $\omega_c$  at each given candidate Doppler value,  $\sigma_D$ , one can proceed as follows:

- 1) Form the two vectors  $\{\tilde{z}_i(\sigma_D, \omega_c)\}_{i=1}^2$ :

$$\tilde{z}_i(\sigma_D, \omega_c) = \text{FFT}(\mathbf{u}_i(\sigma_D)^H \odot \mathbf{y}) \quad (49)$$

Here, we perform an  $M$ -point FFT and, therefore, the candidate values of  $\omega_c$  are given by  $\omega_c^{(m)} = \frac{2\pi(m-1)}{MT_s}$  for  $m = 1, 2, \dots, M$  and gathered in the vector  $\boldsymbol{\omega}_c = 2\pi[0, \frac{1}{MT_s}, \dots, \frac{M-1}{MT_s}]^T$ .

- 2) Evaluate the LLF at all the CFO points in  $\boldsymbol{\omega}_c$  (for the given  $\sigma_D$ ) as follows:

$$\mathcal{L}_y(\sigma_D, \boldsymbol{\omega}_c) = -\log(\psi(\sigma_D)) + \frac{1}{\hat{\sigma}_n^2} \sum_{i=1}^2 \gamma_i(\sigma_D)^2 |\tilde{z}_i(\sigma_D, \boldsymbol{\omega}_c)|^2. \quad (50)$$

Obviously, the new ML estimator, as implemented using the LLF in (50), involves no matrix manipulations (i.e., multiplications or inversions) and, hence, entails a very low computational cost. This is in contrast to the recent ML approach introduced in [46] that requires at each grid point the numerical inversion of a  $(K \times K)$  approximation matrix and  $K$  multiplications of other predefined matrices of the same size. Moreover, in contrast to the simple LLF of (50) which is valid for most common Doppler PSD models (cf. Sections I and II), the ML implementation in [46] relies on a different Taylor series expansion for each Doppler model and, hence, requires its unpractical knowledge *a priori*.

• *Remark 2:* It can be easily verified that, for constant channels (i.e.,  $\sigma_D \rightarrow 0$ ), the new estimator boils down to the very well-known ML frequency estimator proposed in [11]. Indeed, exploiting the fact that  $\lim_{x \rightarrow 0} \sin(Nx)/x = N$ , it follows from (22) and (23) that  $\lambda_1(\sigma_D) \rightarrow 2N$  and  $\lambda_2(\sigma_D) \rightarrow 0$  when  $\sigma_D \rightarrow 0$ . Applying these results in (31), (32), (45), and (46), it can be shown that as  $\sigma_D \rightarrow 0$ :

$$\psi(\sigma_D) \rightarrow 4(1 + N\hat{\rho}), \quad (51)$$

$$\gamma_1(\sigma_D) \mathbf{u}_1(\sigma_D) \rightarrow \sqrt{\frac{\hat{\rho}}{1+N\hat{\rho}}} \mathbf{1}_N, \quad (52)$$

$$\gamma_2(\sigma_D) \mathbf{u}_2(\sigma_D) \rightarrow \mathbf{0}_N. \quad (53)$$

Note here that, in this case, the logarithmic term in the LLF can be dropped as it becomes constant with respect to the CFO parameter. Moreover, using (51)-(53) back in (50) and recalling (49), it follows that (after dropping the constant terms) the LLF of the frequency parameter alone simplifies to:

$$\mathcal{L}_y(\omega_c) \propto |\text{FFT}(\mathbf{1}_N \odot \mathbf{y})|^2 = |\text{FFT}(\mathbf{y})|^2. \quad (54)$$

This means that the ML estimate of the CFO parameter under constant channels is the point that maximizes the discrete Fourier transform of the observation data sequence; a sub-case asymptotic solution compared to ours, yet rightfully appreciated as a major result since it has been established decades ago in the seminal work of Rife and Boorstyn [11].

Recall also that our estimator is built on the two-ray approximation model in (14) that is valid for  $NF_D T_s \ll 1$ . Therefore, for a fixed observation window size ( $N$ ), the proposed estimator suffers from performance degradation at higher Doppler frequencies, more so as the symbol duration increases. In other words, the range of Doppler frequencies over which the basic assumption  $NF_D T_s \ll 1$  remains valid becomes smaller as  $T_s$  gets larger. If the symbol duration is too small, however, this allows one to take more samples and better estimate the Doppler frequency provided that the assumption  $NF_D T_s \ll 1$  is not violated.

#### IV. SIMULATION RESULTS

In this section, we assess the performance of the new ML estimator using the normalized mean square error (NMSE) as a performance metric. In all simulations, the NMSE is computed over  $M = 1000$  Monte-Carlo runs. Main state-of-the-art techniques are selected as benchmarks against which we gauge the performance of the proposed ML estimator. These are:

TABLE I  
CAPABILITIES OF THE DIFFERENT CONSIDERED TECHNIQUES

	Doppler spectrum		Estimated params	
	Model	Robustness	Doppler	CFO
COMAT	Any	No	✓	✓
NLS	Any	Yes	×	✓
AR-ML	<i>uniform Jakes</i>	No	✓	✓
TAML	Any	No	✓	×
<b>New ML</b>	Any	Yes	✓	✓

- The non-linear least-squares (NLS) CFO estimator proposed by Besson and Stoica [20].
- The joint Doppler/CFO ML solution proposed by Abeida and Al Harthi [22]. This estimator is based on the autoregressive (AR) model and, hence, will be simply referred to as AR-ML.
- The ML Doppler estimator proposed by Tsai and Yang [46]. This estimator relies on a time-domain Taylor series expansion of the covariance matrix and it is, hence, referred to hereafter as TAML for time-domain approximate ML.
- The joint Doppler/CFO covariance matching (COMAT) approach proposed by Souden *et al.* [47].

Before delving too much into the simulations details, however, we will compare in Tab. I these techniques with ours (referred to hereafter as “New ML”) in terms of estimation capabilities and robustness. In this context, Tab. I specifies the Doppler spectrum model for which each technique was specifically designed.

From this table, we see that all existing methods but AR-ML apply to any Doppler model yet pending its mandatory *a priori* knowledge, making them little robust in practice. As a matter of fact, only NLS and the new ML approach are completely oblivious to the Doppler spectrum model. Unlike our new ML technique, however, NLS does not estimate the Doppler. Furthermore, although COMAT is the first Doppler estimator to be oblivious in its derivations to the Doppler PSD model, it requires in its implementation an appropriate selection of some correlation lags that could be sensitive to noticeable PSD model mismatches. In light of the above observations from Table I, we will henceforth distinguish the following two estimation scenarios:

- *i)* Joint Doppler/CFO estimation;
- *ii)* Doppler-only estimation with no CFO (i.e.,  $f_c = 0$  Hz).

Under the “joint Doppler/CFO estimation” scenario, we will still benchmark our ML CFO estimator against NLS. Indeed, although the latter does not estimate the Doppler, it does estimate the CFO in spite of an unknown Doppler spread. Under the “Doppler-only estimation” scenario, however, we will discard it along with AR-ML and benchmark the new ML Doppler estimator against COMAT and TAML only. In fact, AR-ML relies on the CFO estimate to find the maximum Doppler shift as follows:

$$\hat{f}_D = \frac{1}{\pi T_s} \sqrt{1 - \gamma(\hat{f}_c)}, \quad (55)$$

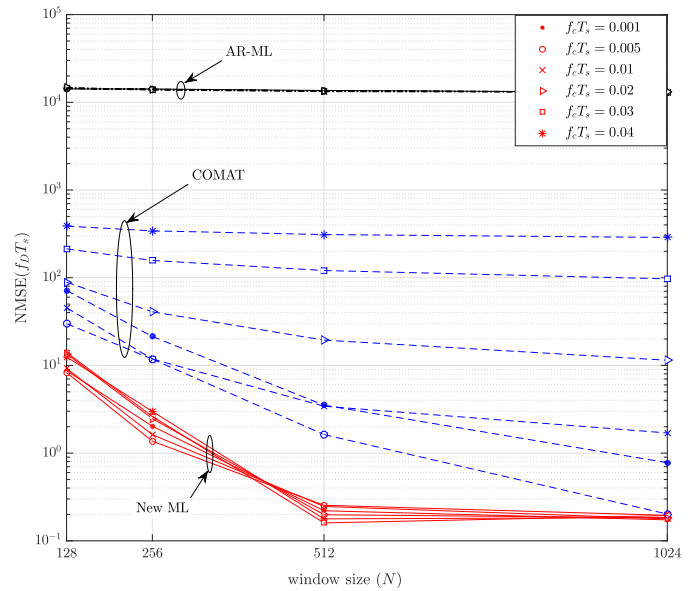


Fig. 1. Doppler NMSE of the various estimators vs. the observation window size ( $N$ ) with  $f_D T_s = 0.002$ , SNR = 0 dB, and *uniform Jakes*’ model.

where  $\gamma(\hat{f}_c)$  is the optimal AR coefficient that is computed from the CFO estimate as shown in [22], eq. (3.11)]. On the other hand, COMAT was modified to account for Doppler-only estimation since its Doppler and CFO estimation tasks can be easily dissociated.

#### A. Joint Doppler/CFO Estimation

In Figs. 1 and 2, we start by studying the effect of the observation window size ( $N$ ) on the performance of the various techniques, respectively, in terms of Doppler and CFO estimation NMSEs. The SNR level is fixed at SNR = 0 dB and we consider the *uniform Jakes*’ model with a normalized Doppler frequency  $f_D T_s = 0.002$ . For  $T_s = 10 \mu s$  (as is almost the case in LTE systems), this corresponds to a maximum Doppler frequency  $f_D = 200$  Hz, thereby translating to a user velocity  $v = \frac{f_D}{F_0} c = 108$  Km/h at a carrier frequency  $F_0 = 2$  GHz.

In Figs. 1 and 2, the proposed ML approach outperforms all the other techniques for all the observation window sizes, except for a slight advantage for COMAT in terms of CFO estimation (for small values of the CFO only) as seen from Fig. 2(a). However, contrarily to COMAT, it exhibits in Fig. 1 a remarkable resilience to the CFO in terms of Doppler NMSE. Whereas AR-ML fails completely at the considered SNR level since it relies on a high-SNR approximation and is not specifically designed to cope with small Doppler values [22]. To support this observation, we plot in Fig. 3 the NMSE performance of AR-ML at a higher SNR value of 30 dB and a higher normalized Doppler frequency  $f_D T_s = 0.008$ . Even if its performance improves appreciably, it can match our new ML estimator only with a large-size observation window of  $N = 1024$ .

Recall here that the proposed estimator relies on the second-order Taylor series expansion in (14) that is valid only when  $N f_D T_s \ll 1$  (cf. Appendix A of [47] for more details).

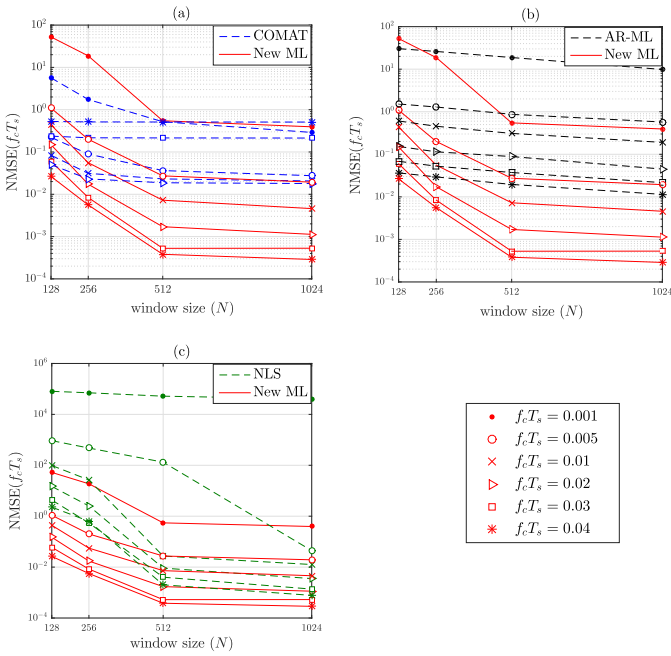


Fig. 2. CFO NMSE of the various estimators vs. the observation window size ( $N$ ) with  $f_D T_s = 0.002$ , SNR = 0 dB, and *uniform Jakes'* model. The New ML estimator is compared to: (a) COMAT, (b) AR-ML, and (c) NLS estimators.

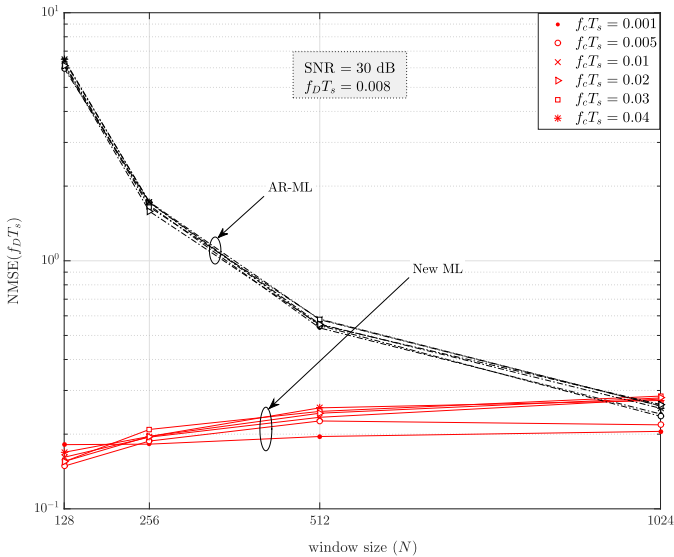


Fig. 3. Doppler NMSE of AR-ML and the new ML estimator vs. the observation window size ( $N$ ) with  $f_D T_s = 0.008$ , SNR = 30 dB, and *uniform Jakes'* model.

Therefore, smaller values for the normalized Doppler frequency,  $f_D T_s$ , allows for larger observation window sizes ( $N$ ) for which the underlying approximation is accurate. This explains why the NMSE of our estimator is decreasing with  $N$  in Fig. 1 while it is increasing in Fig. 3. Indeed, the former corresponds to  $f_D T_s = 0.002$  while the latter corresponds to  $f_D T_s = 0.008$ .

In Figs. 4 and 5, we study the impact of the SNR on the different Doppler and CFO estimators, respectively, at a fixed observation window size  $N = 256$  and  $f_D T_s = 0.002$ . Fig. 5 shows that the proposed ML estimator outperforms

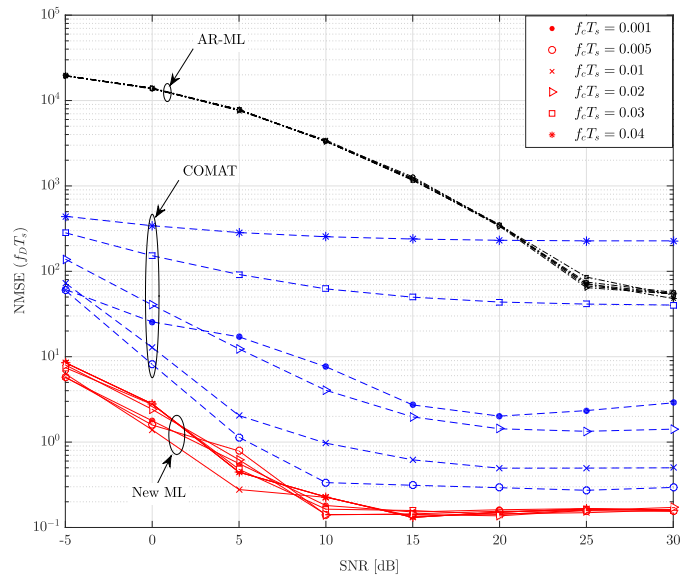


Fig. 4. Doppler NMSE of the various estimators vs. the SNR with  $f_D T_s = 0.002$ ,  $N = 256$ , and *uniform Jakes'* model.

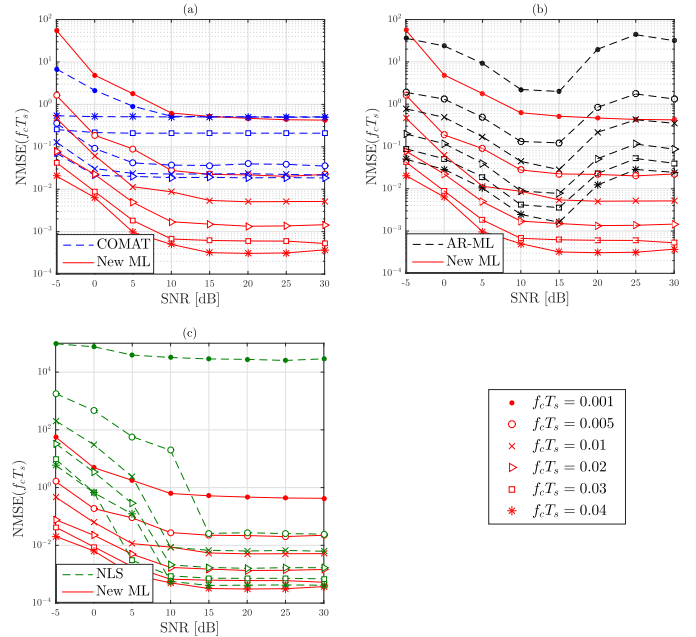


Fig. 5. CFO NMSE of the various estimators vs. the SNR with  $f_D T_s = 0.002$ ,  $N = 256$ , and *uniform Jakes'* model.

the existing techniques in terms of both Doppler and CFO estimation over the entire SNR range, except for a slight advantage for COMAT in terms of CFO NMSE for small CFOs only. Being unable to estimate the Doppler, NLS starts to match our new ML approach in CFO estimation NMSE at relatively increasing SNR values, less so though when estimating relatively larger CFOs as seen from Fig. 5(c).

Figs. 6 and 7 depict the performance of the various estimators as function of the normalized Doppler frequency ( $f_D T_s$ ) under the adverse conditions of low SNR and short data records, namely SNR = 0 dB and  $N = 256$  samples. We observe that the new ML estimator preserves its robustness to the CFO over the entire considered Doppler range. Moreover, although COMAT exhibits a slight advantage in the

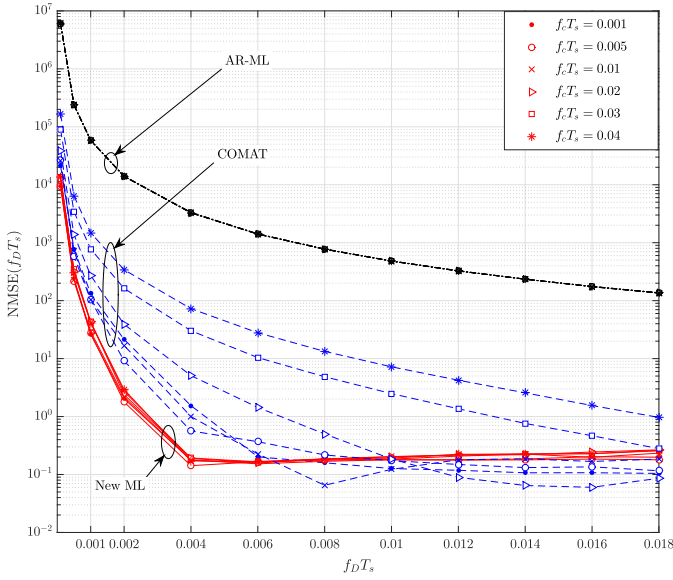


Fig. 6. Doppler NMSE of the various estimators vs. the normalized Doppler frequency ( $f_D T_s$ ) with  $N = 256$ , SNR = 0 dB, and *uniform Jakes'* model.

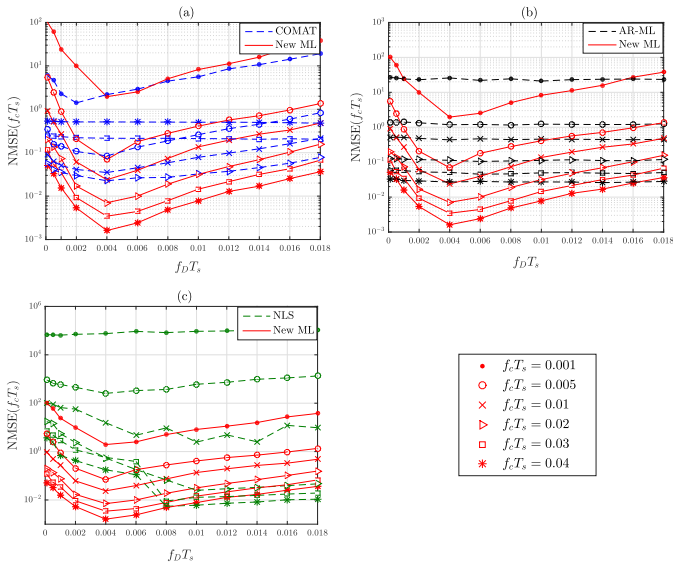


Fig. 7. CFO NMSE of the various estimators vs. the normalized Doppler frequency ( $f_D T_s$ ) with  $N = 256$ , SNR = 0 dB, and *uniform Jakes'* model.

estimation of large Doppler values (at small CFOs though), the new ML estimator outperforms it over the lower end of the Doppler range (i.e.,  $f_D T_s \leq 0.006$ ) that is of most practical interest for high-data-rate systems inherently operating at small values of  $f_D T_s$ . At these low Doppler values, COMAT is, however, more accurate in the estimation of small CFO values. Furthermore, our proposed estimator outperforms AR-ML and NLS over the aforementioned Doppler range of interest at all CFO values.

In Fig. 8, we gauge the performance of the proposed technique against the well-known Cramér-Rao lower bound (CRLB). The latter is a fundamental bound which reflects the best achievable performance theoretically at a given estimation setup. For the sake of clarity, the other estimators

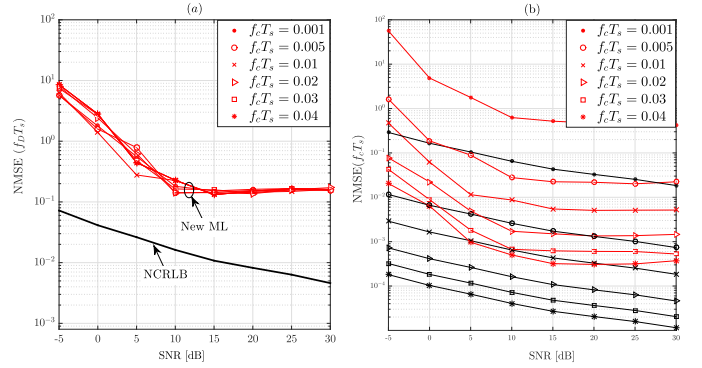


Fig. 8. Comparison of the new ML estimator against the normalized CRLB as function of the SNR with  $f_D T_s = 0.002$ ,  $N = 256$ , and *uniform Jakes'* model, (a) Doppler NMSE and (b) CFO NMSE (black curves are for NCRLB and red curves are for the proposed estimator).

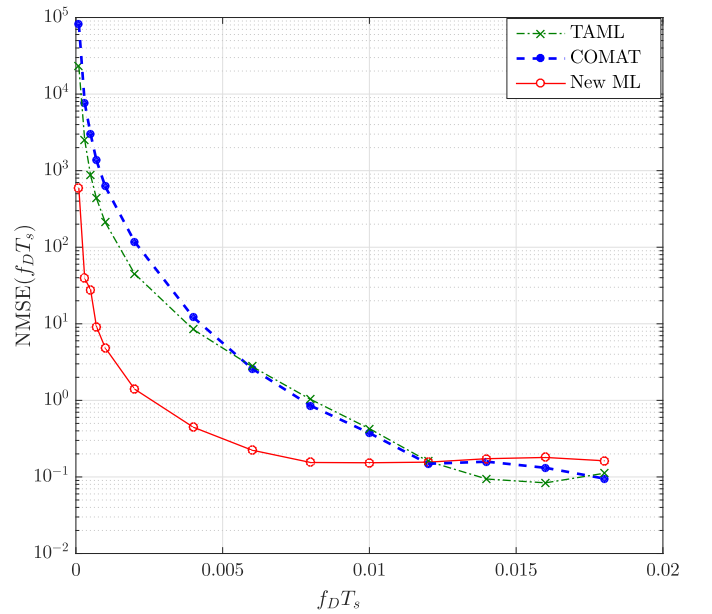


Fig. 9. NMSE of the various estimators vs.  $f_D T_s$  with SNR = 0 dB,  $N = 128$ , and *uniform Jakes'* model.

were not plotted in the same figure. Although the proposed estimator outperforms the existing techniques (as already seen from Figs. 1 to 7), we observe from Fig. 8 that there is room for tremendous performance improvements as predicted by the CRLB.

### B. Doppler-Only Estimation

Fig. 9 shows the NMSE performance of the three estimators (ours, COMAT, and TAML) for an observation window size of  $N = 128$  samples and SNR = 0 dB. The new ML estimator outperforms the other two benchmark techniques over a wide range of the normalized Doppler frequency, (i.e.,  $0.0001 \leq f_D T_s \leq 0.012$ ).

On one hand, COMAT is covariance-based and therefore suffers from a weaker averaging effect at the considered small value of  $N$ . On the other hand, TAML suffers from numerical instabilities due to the numerical inversion of badly conditioned matrices. This can be observed very clearly from the

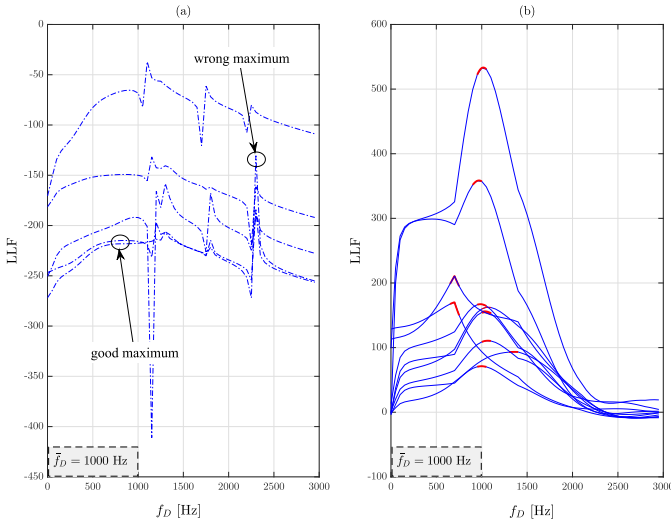


Fig. 10. LLF vs.  $f_D$  for true  $\bar{f}_D = 1000$  Hz, SNR = 0 dB, and uniform Jakes' model for: (a) TAML, (b) New ML.

plots in Fig. 10(a) of different realizations of its approximate LLF for a true<sup>2</sup> Doppler frequency  $\bar{f}_D = 1000$  Hz. There, we see that LLF of TAML, despite exhibiting a true maximum near  $\bar{f}_D = 1000$  Hz, is dominated due to numerical instabilities by another spurious maximum located approximately at  $\bar{f}_D = 2300$  Hz. This is in contrast to the LLF realizations of new ML estimator's LLF plotted in Fig. 10(b), which are always smooth and consistently exhibit a single maximum (cf. red curve segments) near the true Doppler frequency value  $\bar{f}_D = 1000$  Hz.

### C. Complexity Analysis

First, we consider the case of joint Doppler and CFO estimation. We plot in Fig. 11 the computational complexity of our proposed ML-based estimator (New ML) and compare it to that of AR-ML and COMAT. Note that the complexity of our proposed estimator is mainly governed by the FFT size,  $M$ , which dictates the number of candidate CFO values (i.e., the resolution at which we want to estimate the CFO). In Fig. 11, the likelihood corresponding to the new ML estimator was evaluated at  $L = 400$  candidate values for the Doppler. We also considered  $M = 8192 = 2^{13}$  candidate CFO values for both New ML (i.e., its FFT size) and for AR-ML. It is seen that AR-ML is by far the most computationally demanding among all considered estimators. Moreover, although COMAT entails almost the same computational burden at low values of the window size ( $N$ ) as our new ML estimator, the latter has tremendous computational savings over COMAT as  $N$  increases.

In Fig. 12, we also plot the computational complexities for the separate cases of "Doppler-only" and "CFO-only" estimations as function of the window size ( $N$ ). In Fig. 12(a), we compare the new ML estimator to COMAT and TAML while in Fig. 12(b) we compare it to AR-ML, COMAT,

<sup>2</sup>Note here that we use the overbar to distinguish the true value of the Doppler,  $\bar{f}_D = 1000$ , from the generic one (i.e.,  $f_D$ ) used in the  $x$ -axis of Fig. 10

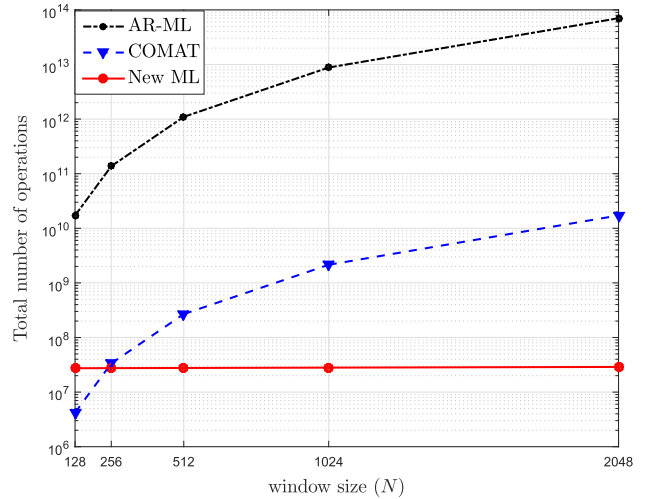


Fig. 11. (Joint Doppler/CFO estimation) Complexities of New ML vs AR-ML and COMAT as function of the observation window size ( $N$ ).

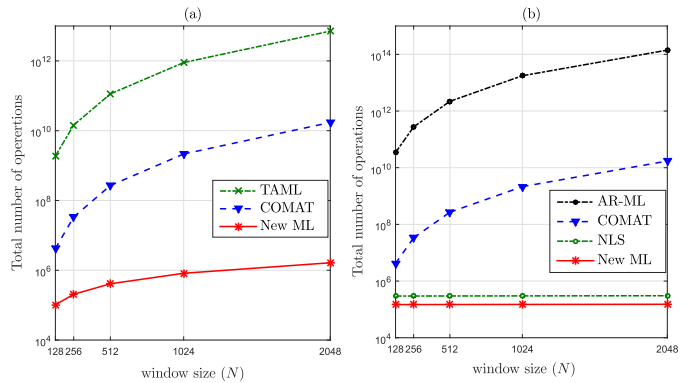


Fig. 12. Complexities vs. the observation window size ( $N$ ) for the cases of: (a) "Doppler-only" estimation and (b) "CFO-only" estimation.

and NLS. As can be seen there, the proposed ML-based algorithm outperforms by far the other Doppler spread estimators in terms of computational complexity. Regarding CFO estimation, however, it entails almost the same complexity as NLS. Yet, it offers a remarkable performance advantage against the latter as already seen in Figs. 2, 5, and 7. Note here that in Fig. 12 (a), we also consider  $L = 400$  candidate Doppler values for both the new ML and TAML. The latter is also implemented using second-order Taylor series expansion. In Fig. 12 (b) the number of candidate CFO values is also fixed at  $M = 2^{13}$ .

### V. CONCLUSION

In this paper, we derived a new approximate ML estimator for the Doppler spread and CFO parameters that is most suitable for current and next generations of high-data-rate wireless communication systems. The new ML estimator is based on an approximation of the channel's covariance matrix by a two-ray model that is valid for most known Doppler PSD models. The likelihood function was recast as the projection onto a two-dimensional subspace and was easily evaluated using the fast Fourier transform (FFT). We showed

via exhaustive computer simulations that the new estimator is accurate over wide ranges of the Doppler spread and CFO parameters. Moreover, it outperforms many state-of-the-art techniques under the adverse conditions of short data records and/or low SNR thresholds. Most prominently, it exhibits an unprecedented robustness to the Doppler spectrum shape of the channel of very practical interest since it does not require its *a priori* knowledge. Yet, the remaining gap between the CRLB and the NMSE of the proposed approximate ML-type estimator suggests that more sophisticated ML approaches need to be derived in order to match the best estimation performance that can be achieved in practice.

## REFERENCES

- [1] F. Bellili and S. Affes, "A low-Cost and robust maximum likelihood Doppler spread estimator," in *Proc. IEEE GLOBECOM*, Atlanta, GA, USA, Dec. 2013, pp. 4325–4330.
- [2] T. Albery and V. Hespelt, "A new pattern jitter free frequency error detector," *IEEE Trans. Commun.*, vol. 37, no. 2, pp. 159–163, Feb. 1989.
- [3] S. Saito and H. Suzuki, "Fast carrier-tracking coherent detection with dual-mode carrier recovery circuit for digital land mobile radio transmission," *IEEE J. Sel. Areas Commun.*, vol. 7, no. 1, pp. 130–139, Jan. 1989.
- [4] X. Cai, Y. C. Wu, H. Lin, and K. Yamashita, "Estimation and compensation of CFO and I/Q imbalance in OFDM systems under timing ambiguity," *IEEE Trans. Veh. Technol.*, vol. 60, no. 3, pp. 1200–1205, Mar. 2011.
- [5] G. Wang, F. Gao, Y.-C. Wu, and C. Tellambura, "Joint CFO and channel estimation for OFDM-based two-way relay networks," *IEEE Trans. Wireless Commun.*, vol. 10, no. 2, pp. 456–465, Feb. 2011.
- [6] K. Cai, X. Li, J. Du, Y.-C. Wu, and F. Gao, "CFO estimation in OFDM systems under timing and channel length uncertainties with model averaging," *IEEE Trans. Wireless Commun.*, vol. 9, no. 3, pp. 970–974, Mar. 2010.
- [7] J. Chen, Y.-C. Wu, S. C. Chan, and T.-S. Ng, "Joint maximum-likelihood CFO and channel estimation for OFDMA uplink using importance sampling," *IEEE Trans. Veh. Technol.*, vol. 57, no. 6, pp. 3462–3470, Nov. 2008.
- [8] J. Chen, Y. C. Wu, S. Ma, and T. S. Ng, "Joint CFO and channel estimation for multiuser MIMO-OFDM systems with optimal training sequences," *IEEE Trans. Signal Process.*, vol. 56, no. 8, pp. 4008–4019, Aug. 2008.
- [9] J. Chen, Y. C. Wu, S. Ma, and T. S. Ng, "ML joint CFO and channel estimation in OFDM systems with timing ambiguity," *IEEE Trans. Wireless Commun.*, vol. 7, no. 7, pp. 2436–2440, Jul. 2008.
- [10] A. A. Nasir, S. Durrani, H. Mehrpouyan, S. D. Blostein, and R. A. Kennedy. (Jul. 2015). "Timing and carrier synchronization in wireless communication systems: A survey and classification of research in the last five years." [Online]. Available: <http://arxiv.org/abs/1507.02032v1>
- [11] D. C. Rife and R. R. Boorstyn, "Single tone parameter estimation from discrete-time observations," *IEEE Trans. Inf. Theory*, vol. 20, no. 5, pp. 591–598, Sep. 1974.
- [12] C. Candan, "A method for fine resolution frequency estimation from three DFT samples," *IEEE Signal Process. Lett.*, vol. 18, no. 6, pp. 351–354, Jun. 2011.
- [13] B. G. Quinn, "Estimation of frequency, amplitude, and phase from the DFT of a time series," *IEEE Trans. Signal Process.*, vol. 45, no. 3, pp. 814–817, Mar. 1997.
- [14] S. Provencher, "Estimation of complex single-tone parameters in the DFT domain," *IEEE Trans. Signal Process.*, vol. 58, no. 7, pp. 3879–3883, Jul. 2010.
- [15] G. Tingting and S. Bin, "A high-speed railway mobile communication system based on LTE," in *Proc. Int. Conf. Electron. Inf. Eng. (ICEIE)*, Kyoto, Japan, Aug. 2010, pp. V1-414–V1-417.
- [16] M. Ghogho, A. Swami, and T. S. Durrani, "Frequency estimation in the presence of Doppler spread: Performance analysis," *IEEE Trans. Signal Process.*, vol. 49, no. 4, pp. 777–789, Apr. 2001.
- [17] Z. Wang and S. S. Abeysekera, "Performance of correlation-based frequency estimation methods in the presence of multiplicative noise," *IEEE Trans. Veh. Technol.*, vol. 55, no. 4, pp. 1281–1290, Jul. 2006.
- [18] W.-Y. Kuo and M. P. Fitz, "Frequency offset compensation of pilot symbol assisted modulation in frequency flat fading," *IEEE Trans. Commun.*, vol. 45, no. 11, pp. 1412–1416, Nov. 1997.
- [19] B. Volker and P. Handel, "Frequency estimation from proper sets of correlations," *IEEE Trans. Signal Process.*, vol. 50, no. 4, pp. 791–802, Apr. 2002.
- [20] O. Besson and P. Stoica, "On frequency offset estimation for flat-fading channels," *IEEE Commun. Lett.*, vol. 5, no. 10, pp. 402–404, Oct. 2001.
- [21] P. Ubolkosold, G. F. Tchere, S. Knedlik, and O. Loffeld, "Simple carrier frequency offset estimators in frequency flat-fading channels," in *Proc. IEEE ICC*, Glasgow, Scotland, Jun. 2007, pp. 2671–2675.
- [22] H. Abeida and M. M. Al-Harathi, "Carrier frequency offset estimation in time-selective Rayleigh flat-fading channels," in *Proc. 21st Eur. Signal Process. Conf.*, Marrakech, Morocco, Sep. 2013, pp. 1–5.
- [23] L. L. He, S. D. Ma, Y.-C. Wu, and T.-S. Ng, "Semiblind iterative data detection for OFDM systems with CFO and doubly selective channels," *IEEE Trans. Commun.*, vol. 58, no. 12, pp. 3491–3499, Dec. 2010.
- [24] H. Nguyen-Le, T. Le-Ngoc, and N. H. Tran, "Iterative receiver design With joint doubly selective channel and CFO estimation for coded MIMO-OFDM transmissions," *IEEE Trans. Veh. Technol.*, vol. 60, no. 8, pp. 4052–4057, Oct. 2011.
- [25] B. Smida, S. Affes, J. Li, and P. Mermelstein, "A spectrum-efficient multicarrier CDMA array-receiver with diversity-based enhanced time and frequency synchronization," *IEEE Trans. Wireless Commun.*, vol. 6, no. 6, pp. 2315–2327, Jun. 2007.
- [26] S. Affes, J. Zhang, and P. Mermelstein, "Carrier frequency offset recovery for CDMA array-receivers in selective Rayleigh-fading channels," in *Proc. IEEE VTC*, Birmingham, U.K., May 2002, pp. 180–184.
- [27] X. Zeng and A. Ghayeb, "Joint CFO and channel estimation for uplink OFDM systems: An application the variable projection method," *IEEE Trans. Wireless Commun.*, vol. 8, no. 5, pp. 2306–2311, May 2009.
- [28] X. N. Zeng and A. Ghayeb, "CFO estimation schemes for differential OFDM systems," *IEEE Trans. Wireless Commun.*, vol. 8, no. 1, pp. 124–129, Jan. 2009.
- [29] D. N. C. Tse and P. Viswanath, *Fundamentals of Wireless Communication*. Cambridge, U.K.: Cambridge Univ. Press, 2005.
- [30] C. Tepedelenioglu, A. Abdi, G. B. Giannakis, and M. Kaveh, "Estimation of Doppler spread and signal strength in mobile communications with applications to handoff and adaptive transmission," *Wireless Commun. Mobile Comput.*, vol. 1, no. 2, pp. 221–242, Jun. 2001.
- [31] G. L. Stüber, *Principles of Mobile Communication*, 2nd ed. Norwell, MA, USA: Kluwer, 2001.
- [32] S. Affes and P. Mermelstein, "A new receiver structure for asynchronous CDMA: STAR-the spatio-temporal array-receiver," *IEEE J. Sel. Areas Commun.*, vol. 16, no. 8, pp. 1411–1422, Oct. 1998.
- [33] S. Lee, K. Sriram, K. Kim, Y. H. Kim, and N. Golmie, "Vertical handoff decision algorithms for providing optimized performance in heterogeneous wireless networks," *IEEE Trans. Veh. Technol.*, vol. 58, no. 2, pp. 865–881, Feb. 2009.
- [34] D. Sandberg, "Method and apparatus for estimating Doppler spread," U.S. Patent 6922452, Mar. 27, 2001.
- [35] J. M. Holtzman and A. Sampath, "Adaptive averaging methodology for handoffs in cellular systems," *IEEE Trans. Veh. Technol.*, vol. 44, no. 1, pp. 59–66, Feb. 1995.
- [36] M. D. Austin and G. L. Stuber, "Velocity adaptive handoff algorithms for microcellular systems," *IEEE Trans. Veh. Technol.*, vol. 43, no. 3, pp. 549–561, Aug. 1994.
- [37] G. Park, D. Hong, and C. Kang, "Level crossing rate estimation with Doppler adaptive noise suppression technique in frequency domain," in *Proc. IEEE VTC-Fall*, Oct. 2003, pp. 1192–1195.
- [38] K. E. Baddour and N. C. Beaulieu, "Robust Doppler spread estimation in nonisotropic fading channels," *IEEE Trans. Wireless Commun.*, vol. 4, no. 6, pp. 2677–2682, Nov. 2005.
- [39] C. Tepedelenioglu and G. B. Giannakis, "On velocity estimation and correlation properties of narrow-band mobile communication channels," *IEEE Trans. Veh. Technol.*, vol. 50, no. 4, pp. 1039–1052, Jul. 2001.
- [40] O. Mauritz, "A hybrid method for Doppler spread estimation," in *Proc. IEEE VTC*, May 2004, pp. 962–965.
- [41] S. Mohanty, "VEPSD: A novel velocity estimation algorithm for next-generation wireless systems," *IEEE Trans. Wireless Commun.*, vol. 4, no. 6, pp. 2655–2660, Nov. 2005.
- [42] H. Hansen, S. Affes, and P. Mermelstein, "A Rayleigh Doppler frequency estimator derived from maximum likelihood theory," in *Proc. IEEE SPAWC*, May 1999, pp. 382–386.

- [43] L. Krasny, H. Arslan, D. Koilpillai, and S. Chennakeshu, "Doppler spread estimation in mobile radio systems," *IEEE Commun. Lett.*, vol. 5, no. 5, pp. 197–199, May 2001.
- [44] A. Dogandi and B. Zhang, "Estimating Jakes Doppler power spectrum parameters using the Whittle approximation," *IEEE Trans. Signal Process.*, vol. 53, no. 3, pp. 987–1005, Mar. 2005.
- [45] *3rd Generation Partnership Project; Technical Specification Group Radio Access Network; Evolved Universal Terrestrial Radio Access (E-UTRA); Physical Channels and Modulation (Release 9)*, document 3GPP TS 36.211, Mar. 2010.
- [46] Y.-R. Tsai and K.-J. Yang, "Approximate ML Doppler spread estimation over flat Rayleigh fading channels," *IEEE Signal. Process. Lett.*, vol. 16, no. 11, pp. 1007–1010, Nov. 2009.
- [47] M. Souden, S. Affes, J. Benesty, and R. Bahroun, "Robust Doppler spread estimation in the presence of a residual carrier frequency offset," *IEEE Trans. Signal Process.*, vol. 57, no. 10, pp. 4148–4153, Oct. 2009.
- [48] J. A. C. Bingham, "Multicarrier modulation for data transmission: An idea whose time has come," *IEEE Commun. Mag.*, vol. 28, no. 5, pp. 5–14, May 1990.
- [49] Z. Wang and G. B. Giannakis, "Wireless multicarrier communications" *IEEE Signal Process. Mag.*, vol. 17, no. 3, pp. 29–48, May 2000.
- [50] K. B. Petersen and M. S. Pedersen. (Nov. 2012). The matrix cookbook, version 20121115. Technical University of Denmark. [Online]. Available: <http://www2.imm.dtu.dk/pubdb/p.php?3274>
- [51] F. Bellili, A. Stephenne, and S. Affes, "SNR estimation of QAM-modulated transmissions over time-varying SIMO channels," in *Proc. IEEE Int. Symp. Wireless Commun. Syst. (ISWCS)*, Reykjavik, Iceland, Oct. 2008, pp. 199–203.
- [52] F. Bellili, R. Meftehi, S. Affes, and A. Stéphenne, "Maximum likelihood SNR estimation of linearly modulated signals over time-varying flat-fading SIMO channels," *IEEE Trans. Signal Process.*, vol. 63, no. 2, pp. 441–456, Jan. 2015.



**Faouzi Bellili** received the B.Eng. degree (Hons.) in signals and systems from the Tunisia Polytechnic School in 2007, and the M.Sc. and Ph.D. degrees (Hons.) from the National Institute of Scientific Research (INRS-EMT), University of Quebec, Montreal, QC, Canada, in 2009 and 2014, respectively. From 2014 to 2016, he was a Research Associate with INRS-EMT, where he coordinated a major multi-institutional NSERC Collaborative Research and Development (CRD) Project on 5th-Generation (5G) Wireless Access Virtualization

Enabling Schemes. He is currently a Post-Doctoral Fellow with the University of Toronto, ON, Canada. He has authored/co-authored over 50 peer-reviewed papers in reputable IEEE journals and conferences. His research focuses on statistical and array signal processing for wireless communications and 5G-enabling technologies.

Dr. Bellili has recently received the very prestigious NSERC PDF Grant Award for the period 2017–2018 and another prestigious PDF Scholarship offered over the same period (but declined) from the Fonds de Recherche du Québec Nature et Technologies. He received the INRS Innovation Award for the year 2014/2015, the very prestigious Academic Gold Medal of the Governor General of Canada for the year 2009–2010, and the Excellence Grant of the Director General of INRS for the year 2009–2010. He also received the award of the best M.Sc. thesis in INRS-EMT for the year 2009–2010 and twice—for both the M.Sc. and Ph.D. programs—the National Grant of Excellence from the Tunisian Government. In 2011, he also received the Merit Scholarship for Foreign Students from the Ministère de l'Éducation, du Loisir et du Sport of Québec, Canada for the period 2011–2013. He was also selected by INRS as its Candidate for the 2009–2010 competition of the very prestigious Vanier Canada Graduate Scholarships Program and for the 2014–2015 competition of the very prestigious Doctoral Dissertation Award of the Northeastern Association of Graduate schools. In 2015, he was also selected by both the University of Waterloo and the University of Toronto as one of their candidates to the very prestigious Banting Postdoctoral Fellowship competition for the year 2015/2016.

He serves regularly as a TPC Member for major IEEE conferences and acts as a Reviewer for many international scientific journals and conferences.



**Yassine Selmi** was born in Tunisia in 1991. He received the B.Eng. degree in telecommunications from the National Engineering School of Tunis, Tunis, Tunisia, and the M.Sc. degree (Hons.) from INRS, Montreal, QC, Canada, in 2015 and 2017, respectively, where he is currently pursuing the Ph.D. degree. His research interests lie in the field of parameters estimation for wireless communications and rapid SDR prototyping of cognitive 5G transceivers.



**Sofiene Affes** (S'94–SM'04) received the Diplôme d'Ingénieur degree in telecommunications and the Ph.D. degree (Hons.) in signal processing from the École Nationale Supérieure des Télécommunications, Paris, France, in 1992 and 1995, respectively. He was a Research Associate with INRS, Montreal, QC, Canada, until 1997, an Assistant Professor until 2000, and an Associate Professor until 2009. From 2003 to 2013, he was a Canada Research Chair in wireless communications. He is currently Full Professor at INRS, and the Director of PERSWADE <[www.create-perswade.ca](http://www.create-perswade.ca)>, a unique CAD 4M Research Training Program on wireless in Canada involving twenty-seven faculty members from eight universities and ten industrial partners. He was a recipient of the Discovery Accelerator Supplement Award twice from NSERC from 2008 to 2011 and from 2013 to 2016. For his contributions to the success of both events, he received the Recognition Award from the IEEE Vehicular Technology Society in 2008 and a Certificate of Recognition from the IEEE Microwave Theory and Techniques Society in 2015. He already served as a General Co-Chair of the IEEE VTC'2006-Fall and the IEEE ICUWB 2015, both held in Montreal, QC, Canada. He is currently serving as the General Chair of 28th IEEE PIMRC to be held in Montreal in the fall 2017. He was an Associate Editor of the IEEE TRANSACTIONS ON WIRELESS COMMUNICATIONS and the IEEE TRANSACTIONS ON SIGNAL PROCESSING. He is an Associate Editor of the IEEE TRANSACTIONS ON COMMUNICATIONS and the *Journal on Wireless Communications and Mobile Computing* (Wiley).



**Ali Ghraryeb** received the Ph.D. degree in electrical engineering from the University of Arizona, Tucson, USA, in 2000.

He was with Concordia University, Montreal, Canada. He is currently a Professor with the Department of Electrical and Computer Engineering, Texas A&M University at Qatar. He is the co-author of the book *Coding for MIMO Communication Systems* (Wiley, 2008). His research interests include wireless and mobile communications, physical layer security, massive MIMO, wireless cooperative networks, and

ICT for health applications. He was a co-recipient of the IEEE Globecom 2010 Best Paper Award.

Dr. Ghraryeb served as an Instructor or a Co-Instructor in technical tutorials at several major IEEE conferences. He served as the Executive Chair of the 2016 IEEE WCNC Conference, and the TPC Co-Chair of the Communications Theory Symposium at the 2011 IEEE Globecom. He serves as an Editor of the IEEE TRANSACTIONS ON COMMUNICATIONS. He has served on the Editorial Board of several IEEE and non-IEEE journals.